Satellite-Based Assessment of Meteorological and Agricultural Drought in Mainland Southeast Asia

Satellite-Based Assessment of Meteorological and Agricultural Drought in Mainland Southeast Asia

Yishan Li, *Student Member, IEEE*, Hui Lu, *Senior Member, IEEE*, Dara Entekhabi, *Fellow, IEEE*, Daniel J. Short Gianotti, *Member, IEEE*, Kun Yang, Caihong Luo, Andrew F. Feldman, *Member, IEEE*, Wei Wang, and Ruijie Jiang

***Abstract*—Satellite-based soil moisture products allow direct monitoring of agricultural drought, especially in regions with sparse ground-based observations. In this study, a soil moisture drought index only based on satellite soil moisture is developed and adopted to assess drought in Mainland Southeast Asia (MSA). We report here on an exceptionally severe Mainland Southeast Asia drought in 2016, which is believed to be strongly linked to the 2015–2016 super El Niño strongly. The event began in February 2016 and lasted until May 2016, with more than 50% of the study areas suffering from moderate drought or worse at peak period. We assess the evolution of agricultural droughts (defined as prolonged deficit in soil moisture) by placing it in the context of the forcing meteorological drought (prolonged deficit in precipitation). The drought assessment using satellite soil moisture is temporally consistent with precipitation-based metrics, but allows for better mapping of the spatial and temporal patterns of how a precipitation deficit may or may not lead to a soil moisture deficit. The specific advantages of a remote-sensing approach—wide-coverage without need for spatially-dense, ground-based climatological records, and sensitivity to otherwise unmeasured irrigation inputs—suggest further opportunity for drought monitoring in ungauged regions, particularly in agricultural contexts.**

Manuscript received 12 May 2022; revised 21 June 2022; accepted 3 July 2022. Date of publication 13 July 2022; date of current version 9 August 2022. This work was supported in part by the National Key Research and Development Program of China under Grant 2017YFA0603703, in part by the Second Tibetan Plateau Scientific Expedition and Research Program STEP, under Grant 2019QZKK0206, in part by the National Natural Science Foundation of China under Grants 91747101 and 41801260, in part by the Strategic Priority Research Program of Chinese Academy of Sciences under Grant XDA20100300, in part by the Tsinghua National Laboratory for Information Science and Technology and in part by the China Scholarship Council under Grant 201906210100 for international cooperation. *(Corresponding author: Hui Lu.)*

Yishan Li is with the Department of Earth System Science, Tsinghua University, Beijing 100084, China, also with the Department of Civil and Environmental Engineering, Massachusetts Institute of Technology, Cambridge, MA 02139 USA, and also with the Chongqing Ecological Environment Bureau, Chongqing 401120, China (e-mail: liys15@mails.tsinghua.edu.cn).

Hui Lu, Kun Yang, and Ruijie Jiang are with the Ministry of Education Key Laboratory for Earth System Modeling and the Department of Earth System Science, Tsinghua University, Beijing 100084, China, and also with the Ministry of Education Ecological Field Station for East Asian Migratory Birds, Beijing 100084, China (e-mail: luhui@tsinghua.edu.cn; yangk@tsinghua.edu.cn; jrj20@mails.tsinghua.edu.cn).

Dara Entekhabi, Daniel J. Short Gianotti, and Andrew F. Feldman are with the Department of Civil and Environmental Engineering, Massachusetts Institute of Technology, Cambridge, MA 02139 USA (e-mail: darae@mit.edu; gianotti@mit.edu; afeld24@mit.edu).

Caihong Luo is with the Chongqing Ecological Environment Bureau, Chongqing 401120, China (e-mail: 1415582725@qq.com).

Wei Wang is with the Changjiang Institute of Survey, Planning, Design and Research, Wuhan 430010, China (e-mail: weiwang08thu@gmail.com).

This article has supplementary downloadable material available at https://ieeexplore.ieee.org, provided by the authors.

Digital Object Identifier 10.1109/JSTARS.2022.3190438

***Index Terms*—Agricultural drought, drought monitor index, Mainland Southeast Asia (MSA), meteorological drought, SMAP.**

I. Introduction

DROUGHT is a persistent threat to economic, hydrologic, environmental, and agricultural systems, and has rapidly changing forms, costs, and scopes [1]–[3]. The intensity and extent of droughts tend to increase as they transform from being precipitation deficits (meteorological drought) to soil moisture deficits (agricultural drought), which eventually leads to water storage depletion in aquifers and surface water bodies and reduces the flows of streams and ecosystems (hydrological drought) [2], [4]. Human society is being affected by increasing drought occurrences [4]–[6].

The quantification of drought impacts is often limited by drought metrics and methods. To determine drought conditions within a period [7], many agricultural drought assessment methods are primarily based on the statistical characteristics of long-term meteorological data and meteorological drought function, rather than being focused on key system variables. For example, agricultural systems often experience the persistent effects of precipitation, evaporation, and temperature for months and years beyond the "official" duration of a specific drought event [8], [9]. Since drought-related variables (such as precipitation, temperature, soil moisture, and runoff and discharge) are based on different variables, multiple drought indices have been developed [10]. However, most of them characterize meteorological drought, and few indices can monitor agricultural drought directly derived from soil moisture observations. The most commonly used agricultural drought index, the crop moisture index (CMI), is based on the well-known meteorological drought index: the Palmer drought severity index (PDSI) [11], [12]. Both CMI and PDSI require more than one meteorological variable as input, such as precipitation, temperature, and soil moisture. The empirical standardized soil moisture index (ESSMI) is based on a subset of the standardized precipitation index (SPI), an index widely used in the detection of meteorological drought and abnormal precipitation [13], [14]. Two weekly indices, the soil moisture deficit index and the evapotranspiration deficit index, were developed based on simulated data derived from the soil and water assessment tool (SWAT) for agricultural drought monitoring [15]. Similarly, the soil moisture drought severity index, which is based on the monthly output of the community

land model, was developed in 2015 to assess the drought area and related trends in North China [16]. Conversely, based on reality reference crops, the agricultural reference index for drought was developed to quantify drought and its effects on crop yields [17].

Soil moisture can reflect recent precipitation and antecedent conditions and indicate imminent water shortage and agricultural drought risk. Therefore, soil moisture profile monitoring is vital for assessing agricultural drought and preventing the subsequent impact of severe drought events [18]. Remotely-sensed soil moisture data from recent satellite missions (AMSR-E [19]; SMOS [20]; SMAP [21]; AMSR-2 [22]) provide direct agricultural drought observations, without the spatial representation errors of in situ soil moisture sensors or the process errors of land surface models [23]–[25]. Although retrieval methods and land-cover types cause satellite soil moisture errors, present studies have demonstrated that satellite-based soil moisture is able to derive relatively accurate assessments of drought stress at continental to global scales without in situ observations [26]–[29]. This demonstrates the role of soil moisture as the intermediary between meteorological drought and lagged vegetation productivity indices [7], [30]. Therefore, soil moisture dynamics, which is an indicator that includes precipitation and evapotranspiration and is directly related to vegetation growth status, has the potential to be used as a source for agricultural drought monitoring. Furthermore, information on precipitation, evapotranspiration, vegetation, and land cover type is difficult to obtain in many undeveloped areas globally. Assimilating satellite-based observations to land surface models is a viable option for obtaining information on vegetation condition and root-zone soil moisture [31]–[34], and for assessing agricultural and drought conditions; however, the results tend to include errors from the model calculation process. Monitoring agricultural drought solely through the remotely-sensed observations of soil moisture and rapidly detecting the disturbance of precipitation, irrigation, and other water cycle processes are important for agriculture, particularly in regions that rely on agriculture but have a paucity of meteorological data.

In this study, we propose a drought monitor index based on daily to 8-day soil moisture observations [soil moisture drought eight day index (SED)] to monitor the agriculture drought in regions lack of meteorological data, which is only driven by satellite soil moisture retrievals with no land surface or hydrological modeling. SED incorporates the advantages of remote sensing, with characteristics such as a large-scale coverage, high temporal and spatial resolutions, and ability to perform direct observations, thereby compensating for disadvantages, such as lack of historical data. Unlike drought indicators based on long-term historical data that characterize the level of water-related variables relative to the historical period, SED characterizes the level of root-zone soil moisture deficit in the short term (subyear) and can reflect the actual agricultural drought situation in the short term. Furthermore, the input data of SED is the root-zone soil moisture calculated from the surface soil moisture, and the calculation of root-zone soil moisture can be adjusted according to the different crop types in different regions, enabling SED to meet the actual situation of the study area.

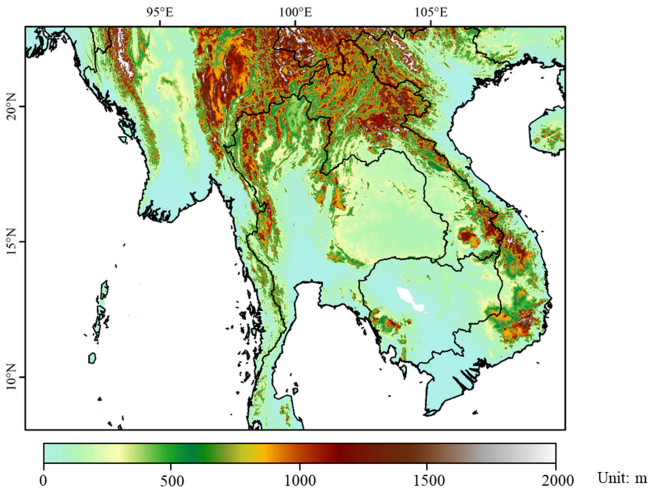

Fig. 1. Study area elevation, with mountain ranges in the north, plains in the south, and Tonle Sap Lake, the largest freshwater lake, located in Cambodia.

II. Study Area

We focus on Mainland Southeast Asia (MSA), which spans the latitude range 8° N to 23° N and longitude range 90° E to 110° E (see Fig. 1). This region predominantly comprises five countries: Cambodia, Laos, Myanmar, Thailand, and Vietnam; these countries are primarily drained by the Irrawaddy, Chao Phraya, and Mekong rivers. MSA has significant relief, with altitudes ranging from −200 m to 3000 m; it supports a variety of forested and agricultural landcovers, with noted orographic effects on hydroclimate [35], [36]. Precipitation in the region is strongly influenced by the East Asian Monsoon regimes of enhanced moisture advection from the Bay of Bengal in the Northern Hemisphere summer (late May to September), and cold dry conditions in the winter (November to March) [37], [38]. The countries in MSA have a population of approximately 240 million, with agriculture comprising a large portion of both individual livelihoods and national-level gross domestic products [39]–[42].

However, much of MSA has become and will continue to be increasingly vulnerable to drought because of projected reductions in precipitation, rise in air temperature and evapotranspiration, and increasing population demands on water resources from all sectors, with all these impacts being dependent on transboundary management strategies [43], [44]. Drought hazards are known to have caused serious losses in this region [45], [46], and droughts within the Lower Mekong River Basin (LMB) have been of longer durations and more severe in recent decades [47]. Food security and ecosystem services in the region show a significant dependence on water resources [44], [48].

III. Data and Methodology

A. Satellite-Based Soil Moisture Data

Satellite-based soil moisture data from the SMAP Enhanced Level 3 soil moisture product (SPL3SMP_E) [49] was used to

generate the root-zone soil moisture, which was the only input to the SED. The SMAP satellite was launched by NASA in January 2015 to acquire global mapping of soil moisture from space via brightness temperature measurement, and provides global coverage every three days. The satellite now carries a passive *L*-band radiometer (1.41 GHz) that allows us to obtain surface soil moisture data (nominally volumetric water content within the top 5 cm of the soil column) at a 36 km resolution (half-power definition) [21]. The SPL3SMP_E product contains both descending and ascending radiometer-based soil moisture retrievals gridded at a resolution of 9 km. The descending data between 1 April 2015 and 31 March 2020 were selected to calculate SED. We performed the analyses at an 8-day resolution to make use of the exact eight-day revisit pattern of the SMAP instrument, thereby eliminating potential sampling discrepancies for spatial analysis.

B. Climate Data

The modern-era retrospective analysis for research and applications version 2 is produced by NASA's Global Modeling and Assimilation Office, which has an integrated Earth system analysis capability that couples the atmosphere, ocean, land, and chemistry systems [50]. In this study, 20 years of data (2000–2019) were used for the meteorological drought analysis and comparison with SMAP retrievals. Precipitation from the single-level diagnostics (M2T1NXSLV) dataset was used at a spatial resolution of 0.5° × 0.5° to illustrate meteorological drought characteristics.

C. Additional Datasets

We determined areas with irrigation potential using a global map of irrigated areas from the UN Food and Agriculture Organization (FAO) [51].

To determine topographic influence on drought and precipitation fields, we used a digital elevation model from the NASA shuttle radar topographic mission at a resolution of approximately 90 m [52].

D. Development of SED

Croplands and vegetated ecosystems respond to water availability integrated over their root profiles [53], [54], thereby showing drought responses that are somewhat lagged and dampened relative to the uppermost surface layer. Owing to the conductive and capillary processes, surface soil moisture is both physically and statistically related to root-zone soil moisture [55], which allows us to use remotely sensed surface soil moisture to estimate root-zone soil moisture [56], [57].

$$\mathrm{RZSM}\,(t_n) \;=\; \frac{\sum_i^n \mathrm{ms}\,(t_i)\, e^{-\frac{t_n - t_i}{T}}}{\sum_i^n e^{-\frac{t_n - t_i}{T}}} \tag{1}$$

where $\mathrm{RZSM}(t_n)$ is the rootzone soil moisture at time t_n, $\mathrm{ms}(t_i)$ is the satellite soil moisture at time t_i, t_i represents the time of the ith measurement, and T is the time scale parameter representing the scale at which surface soil moisture affects root-zone soil moisture. After calibration on MSA, the drought condition for different T values (from 15 days to 65 days) was obtained; $T =$ 55 days was applied in this study.

The root-zone soil moisture was then used to fit the Beta distribution in a 180-day window (+/−90-day around moment t_n) and determine the shape parameters of the beta distribution at moment t_n grid-by-grid. The 180-day window allows for a sufficient sample size to perform statistical estimation, while the moving window captures seasonality. The shape parameters in this study were dynamic, thereby varying with seasons and soil moisture within the fitting window; the dynamic characteristics also gave SED the ability to sensitively monitor short-term changes in soil moisture. Finally, SED at t_n was classified in terms of the percentile of $\mathrm{RZSM}(t_n)$ in the corresponding beta probability density curve.

The beta distribution is a continuous probability distribution defined between limits *a* and *b* with two positive shape parameters (α and β), with the flexibility to assume a wide variety of shapes. Many studies and applications (including the study of drought) have applied the beta distribution, especially for data within finite intervals

$$f\;(\mathrm{RZSM};\alpha,\beta) = \frac{(\mathrm{RZSM}-a)^{(\alpha-1)}(b-\mathrm{RZSM})^{(\beta-1)}}{B\,(\alpha,\beta)\,(b-a)^{\alpha+\beta-1}} \quad \text{where } a \le \mathrm{RZSM} \le b,\ \alpha,\ \beta\ > 0 \tag{2}$$

where α, β are the shape parameters, and *a*, *b* are the bounds of the distribution [29]. Here, $a = 0$ corresponds to a fully desiccated soil, while the upper bound *b* is the soil porosity of each pixel (in the range of 0.3–0.6). Soil porosity represents the pore space of soil containing the liquid and gas phases, which could be the upper limit of soil moisture. When soil moisture reaches *b*, it implies that all the space in the soil is filled with water and the value of *b* is the upper limit of soil moisture physically. $B(\alpha,\beta)$ is a beta standardized function, $B\;(\alpha,\beta) = \int_0^1 t^{\alpha-1}(1-t)^{\beta-1}dt$, which is used to make the probability density integral to this distribution equal to 1. The samples before and after 90 days of a specific date were grouped and input to determine the parameters α and β at each pixel. After determining the parameters α and β, the SED were classified according to the percentile of different soil moisture values in the respective distribution curve. Based on beta fitting, a continuous distribution curve was fitted for each grid on each day within a 180-day moving window. With the continuous curve, the percentile of soil moisture within the fitted window was determined, and the drought level of each day could be classified. Although the retrieval period of SPL3SMP_E is 2–3 days, the sweeping style of SMAP satellite does not guarantee that observations are available for every pixel in the whole MSA for a given 3-day period. Therefore, to ensure the most weighted observation data of drought maps from satellite observation, an 8-day mapping period was chosen for this study, which guaranteed that each pixel in the mapping period contained at least one observation [58]–[60]. Finally, the 8-day average root-zone soil moisture was used to calculate percentile and complete the agricultural drought mapping. Fitting soil moisture to beta distribution has been widely used in studies and has been shown to be reliable

TABLE I
DROUGHT DEFINITIONS FOR SED AND SPI-1

Category	SED Percentile	SPI Ranges	SED Input	SPI Input
Abnormally Dry	30%	–0.5 – –0.7	Soil Moisture	Precipitation
Moderate Drought	21%	–0.8 – –1.2	SED Distribution	SPI Distribution
Severe Drought	11%	–1.3 – –1.5	Beta	Gamma
Extreme Drought	6%	–1.6 – –1.9	SED Temporal Resolution	SPI Temporal Resolution
Exceptional Drought	3%	<–0.2	8-day	Monthly

[28], [29], [61], and the beta-fitting of short-term root-zone soil moisture in this study further highlights the response of agricultural drought after being disturbed by soil moisture.

E. Standard Precipitation Index

SPI is a drought index based on the probability distribution of long-term historical precipitation data [14] and reflects unusual dryness or wetness over a region at different time scales that are often 1, 3, 6, 12, or 24 months. The central idea of SPI is to transform accumulated precipitation totals to a standard normal distribution, with a standard deviation of 1 and mean of 0 (typically as CDF-mapping from a gamma distribution). Different time scales are used for different hydroclimate analyzes.

Twelve-month and greater scale accumulations are usually used to assess decadal variability, 3-month and 6-month accumulations are used for multiyear drought assessment, and 1-month accumulations are used for short period dry-wet condition monitoring. Given the temporal resolution and the input data of SED on a 1–2 month scale, 1-month SPI (SPI-1) was introduced in this study to validate the trends in drought onset and changes detected by SED. SPI-1 is a meteorological drought indicator at a monthly scale, which focuses on the relative abundance of precipitation for each month and reflects a relative dryness and wetness state over the period for which precipitation data are available. Compared with other scales of SPI, SPI-1 is the most sensitive meteorological drought indicator for precipitation in the short term and is closer to the sensitive response of SED to precipitation.

Table I shows the classification percentile and cumulative distributions associated with SED and SPI-1. The SED and SPI are classified into five categories according to the U.S. drought monitoring system.

IV. RESULTS

We present our results in the following four main sections:

1) the selection of time scale parameter T;
2) the temporal evolution of drought over the region, based on time series of SPI-1 and SED;
3) a case study comparing springtime drought conditions in 2016;
4) a point-to-point comparison of SPI and SED to determine agricultural drought information encoded in root-zone soil moisture (beyond that in SPI);
5) the transition from meteorological drought to agriculture drought.

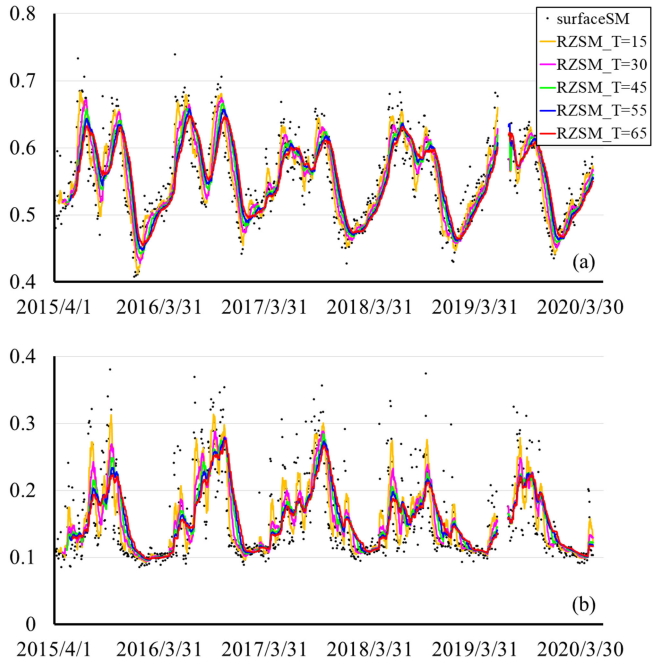

Fig. 2. Surface and root-zone soil moisture of two pixels, with (a) located in the Mekong River Delta with wet conditions and (b) located in central Myanmar with dry conditions.

A. Time Scale Parameter T

Time scale parameter T is only parameter that can be adjusted in the exponential filter method for generating root-zone soil moisture, and is used to determine how long scales of surface soil moisture can influence root-zone soil moisture. Previous studies have confirmed the feasibility of calculating root-zone soil moisture using the exponential filter method, and have discussed the choice of parameter T [62]–[66]. These studies also suggested that different soil types, porosity, and depth affect the value of T [56], [57], [65].

Fig. 2 demonstrates the surface and root-zone soil moisture of two example points. Fig. 2(a) represents a wet condition, with an average soil moisture of 0.55 in the Mekong River Delta in southern Vietnam. Fig. 2(b) represents a dry condition, with an average soil moisture of 0.16 in central Myanmar. For both dry and wet conditions, the root-zone soil moisture calculated by the exponential filter method follows the changes in surface soil moisture; there is little difference in the magnitude and trend of the soil moisture when T changes from 15 to 65 days. Furthermore, the variation of the root-zone soil moisture curve becomes significantly smaller as T increases, and there are more significant soil moisture fluctuations within 10-day scales (soil moisture change of more than 0.05 within 10 days and rapid recovery) at $T = 15$. The vegetation had some tolerance to

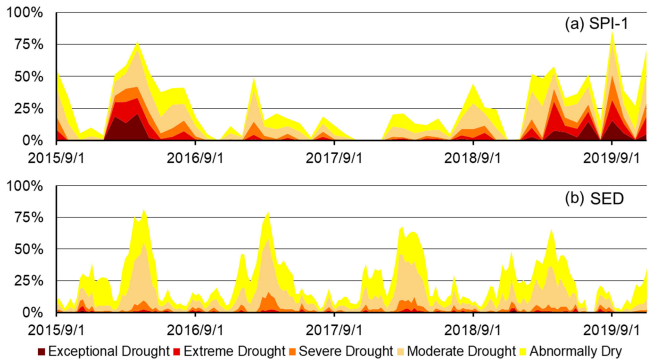

Fig. 3. Percent meteorological drought (SPI-1) and agricultural drought (SED) area of MSA, showing that (a) percent area of monthly SPI-1 detected a long-term exceptional drought in 2016 and (b) percent area of 8-day SED also detected a severe drought from the 2015 winter to the 2016 spring.

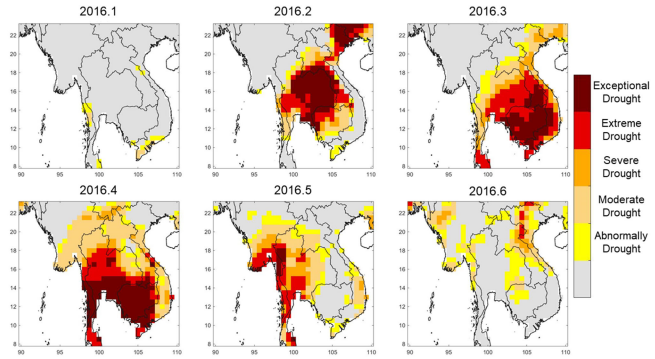

Fig. 4. SPI maps of the 2016 spring drought event. Meteorological drought based on SPI begins in February 2016 in Thailand and Northern Vietnam, migrates south to Cambodia and Southern Thailand in March and April, and mitigates from east to west in May.

soil moisture changes and was able to offset some soil moisture variation.

For soil depths ranging from 0 to 25 cm, the general choice for T is approximately 20 days; for deeper soils, T increases. According to information from the FAO, the main agricultural product grown in the study area is maize, with a root depth distribution exceeding 100 cm [67], [68]. According to previous studies, $T = 60$ days is the optimal choice for soil depths of 50–100 cm [63]. Therefore, when considering the crop type and reducing the fluctuation of soil moisture, $T = 55$ days is set in this study.

B. Temporal Evolution of Drought in MSA

The temporal evolution of meteorological and agricultural drought conditions across the entire study area is shown in Fig. 3, as captured by the 8-day SED and monthly SPI-1 metrics. In each panel, the colors denote the fraction of the study area determined at each drought classification for a given time. The darker the color, the more severe the drought; the fraction represents the percentage of drought area in the total mainland area. All the metrics follow similar patterns, with a more intense drought being detected annually or semi-annually from 2015 to 2019. The fraction of drought area percentage ranges from 0% to 80%, and the 8-day SED curve suggests less exceptional drought area in drier years such as 2016 and 2019. Both curves detect the drought that occurred in 2016 spring, which was a severe drought event with extreme severity, long duration, and large spatial coverage. SED exhibits periodic drought somewhere in the study region in every dry season; the difference between the dry season and the wet season is evident, while the performance of SPI is significantly different (with interannual variability). Therefore, the two curves of the drought situation in 2017 and 2018 do not match. The drought percentage area in the dry season is less than that in the wet season. This is because SPI mainly reflects the current status of precipitation in the 20-year historical period rather than the recent real dry or wet condition, while the SED describes interannual, short-term relative changes in wet and dry conditions. The year-to-year differences it demonstrates are also formed by the extension of short-term changes in drought conditions, rather than the differences between one year (or months) and the multiyear averages (as in the SPI).

C. Meteorological Drought to Agriculture Drought in 2016

During the study period, the spring 2016 drought had the highest percentage of meteorological and agricultural drought area (at more than 75%). It was also a severe meteorological drought as suggested by SPI and was the most severe drought over MSA in the 2015–2019 period. According to the Mekong River Commission and Ministry of Water Resources of China [69], the drought in 2016 caused considerable damage to agricultural production in the region and affected the living conditions and livelihoods of the people living along rivers. We mapped the spring 2016 drought map from the perspectives of SPI and SED. The monthly SPI maps from January to March in 2016 are shown in Fig. 4. The meteorological drought event commenced in February when nearly half of the region suffered from moderate or severe drought, after which the event intensified and resulted in more than 75% pixels experiencing drought in April (before eventually mitigating in May). Correspondingly, Fig. 5 demonstrates the 8-day agricultural drought maps based on SED. Unlike the meteorological drought detected by SPI that appeared suddenly in February, the higher temporal resolution from SED shows the process of the 2016 spring drought to be more serious and widespread. The drought commenced on February 21st over the northwestern region and then migrated to the middle of MSA, causing widespread drought from 24th March to 25th April. Similarly, the drought indicated by SED began to subside in May, and also persisted in western regions, such as the Irrawaddy Delta. At the end of the 2016 spring drought, the SED maps change rapidly following precipitation triggered by the summer monsoon.

D. Submonthly Characteristics of SED

Here, we show some characteristics of SED and display the advantages of these characteristics by comparing SED with SPI. Currently, indicators that are widely applied in drought research have different limitations:

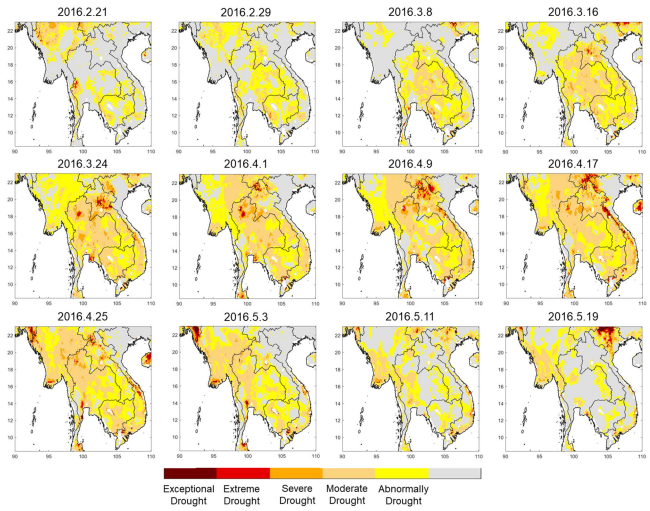

Fig. 5. SED maps of the 2016 spring drought event. Agricultural drought based on SED begins in late February, spreads to most of the study area in March and April, and mitigates from east to west by May.

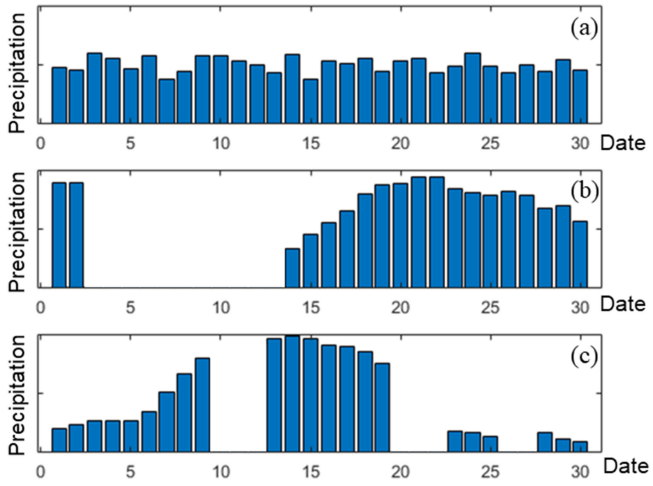

Fig. 6. Example of different sub-monthly precipitation patterns. (a) Relatively balanced case of precipitation, with an expectation of smooth root-zone soil moisture, (b) case precipitation concentrated at the end of the month, with root-zone soil moisture expected to decrease significantly at the beginning of the month, and (c) Cases with fluctuating precipitation in the month, when root-zone soil moisture may also fluctuate.

1) Coarse time scales. For example, SPI and PDSI [70] are used monthly; the submonthly characteristics of precipitation occurrence and intensity can have major effects on soil moisture state and runoff [55], leading to significantly divergent agricultural drought conditions, even with identical SPI.
2) Based on long historical data. Existing indicators typically reflect relative wet and dry conditions based on long-term historical data rather than near real-time conditions, such as SPI and ESSMI.
3) Requiring more input data. Such as PDSI and CMI require precipitation, temperature, and soil moisture as input.

These limitations are critical to drought monitoring in MSA, where observation gauges are uneven and long-term meteorological data are difficult to obtain. Fig. 6 shows three simulated precipitation time series, all of which have the same monthly accumulated precipitation, but different daily distributions. Fig. 6(a) represents the precipitation status, where root-zone soil moisture can remain sufficient. Fig. 6(b) and (c) presents an uneven monthly distribution of precipitation, where root-zone soil moisture will change over time with different characteristics. The same monthly precipitation results in the same SPI, while different daily precipitation forcing time-series patterns result in different root-zone soil moisture time series. However, the SPI cannot detect the differences.

This inability to resolve differing precipitation deficit time patterns can be shown with observations. Fig. 7 shows SPI-1 and SED time series estimated based on observations for three pixels. For each pixel, two SPI-1 values are highlighted with nearly identical magnitudes (inverted triangle symbols in each of Fig. 7(b)–(d); different values for each pixel but the same value within the time-series of each pixel). In each case, the matching SPI-1 values correspond to SED values in different drought classes. This is because of the impact of precipitation timing at submonthly scales on agricultural (root-zone soil moisture state) drought. More recent precipitation events will typically have more impact on the current root-zone soil moisture state; however, physical hydrological dynamics vary from location to location and can be highly nonlinear with (nonprecipitation) variables, implying that observable root-zone soil moisture states will likely always represent agricultural drought conditions better than aggregated precipitation. The SMAP product is a result of physical hydrological dynamics processes; its soil moisture experienced rainfall, vegetation canopy interception, infiltration, and vegetation transpiration.

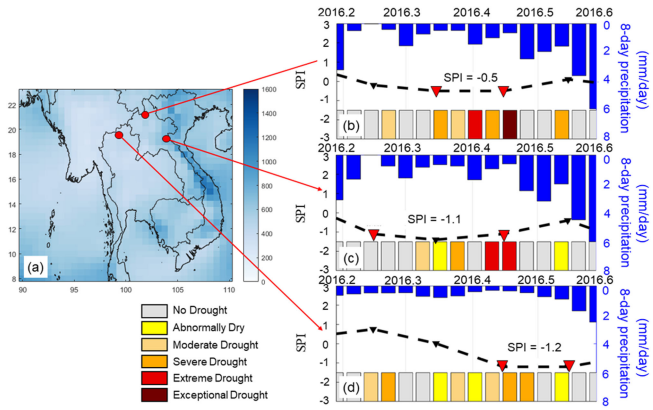

Fig. 7. Impact of precipitation timing on drought definition, showing (a) average precipitation map of 2016 spring drought period, and location of three highlighted pixels, (b) time series of 8-day precipitation (blue bars), monthly SPI-1 (dashed line with triangular markers), and 8-day SED values (uniform height bars) for a location in northern Laos, (c) time series of 8-day precipitation (blue bars), monthly SPI-1 (dashed line with triangular markers), and 8-day SED values (uniform height bars) for a location in central Laos, (d) time series of 8-day precipitation (blue bars), monthly SPI-1 (dashed line with triangular markers), and 8-day SED values (uniform height bars) for a location in northern Thailand. In each case, pairs of similar SPI-1 values correspond to very different SED values, highlighting the role of precipitation timing on agricultural drought.

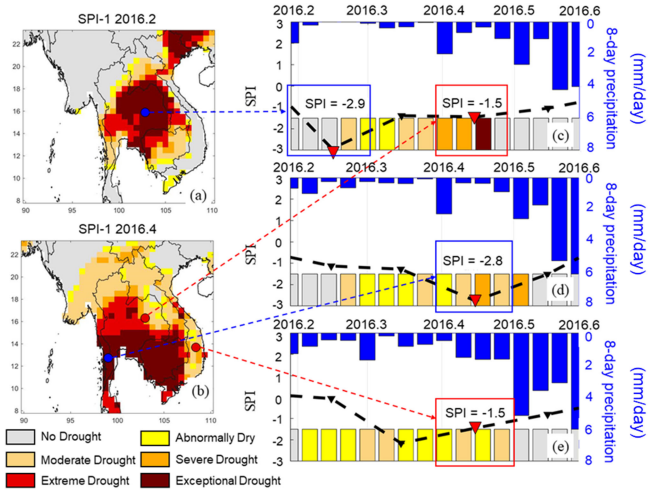

Fig. 8. Demonstrating that SPI-1 and SED do not translate across space. (a) SPI-1 map of February 2016. (b) SPI-1 map of April 2016. (c)–(e) Time series of 8-day precipitation (blue bars), SPI-1 (dashed lines and triangular markers), and SED (uniform height bars) for three locations shown in (a) and (b). Blue boxes in (c) and (d) both have SPI-1≈ -2.9, but mean SED = abnormally dry in (c) and mean SED = mild drought in (d). Red boxes in (c) and (e) both have SPI-1≈ -1.5, but mean SED = severe drought in (c) and mean SED = moderate drought in (e).

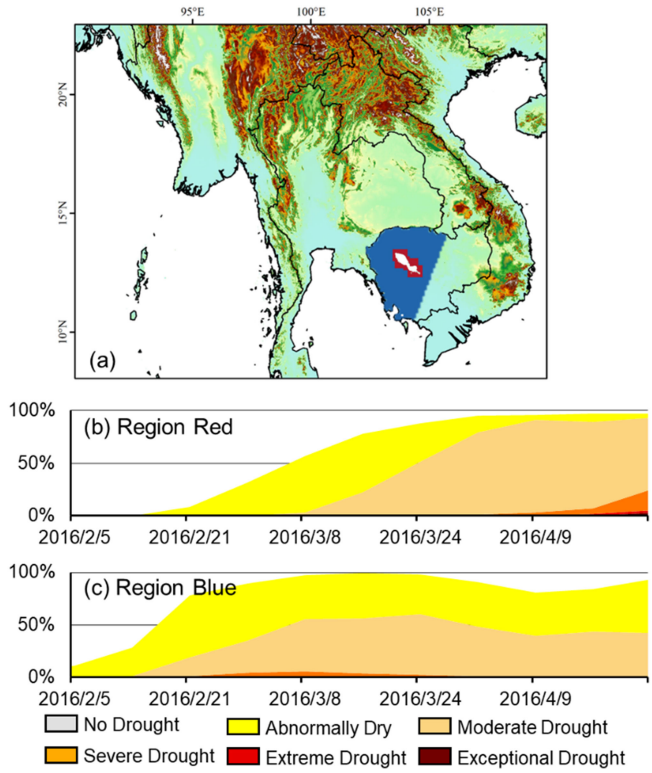

Fig. 9. Drought area percentage of Eastern Cambodia and Western Cambodia. Red area is the region close to Tonle Sap Lake, blue area is the region around Tonle Sap Lake but farther away. (a) Delineation of the two regions and (b) and (c) time series of drought percentage area of the two regions. The drought in the red area is one month later than the drought in the blue area.

Therefore, it can be regarded that the SMAP product has considered the factors that influence the physical hydrological dynamics processes, such as topography and soil texture.

Although they are both relative metrics, SPI and SED values do not necessarily correspond across space. Fig. 8(a) and (b) shows the SPI values for February and April 2016, respectively. The time series of 8-day precipitation, SPI, and SED are shown for three locations [see Fig. 8(c) and (d)]. The February SPI for a location in northern Thailand [see Fig. 8(c)] is similar to the April SPI for a location in southern Myanmar [see Fig. 8(d)], but corresponds to very different SED values (Abnormally Dry versus moderate drought). The April SPI from the same northern Thailand location is very similar to the April SPI for a location in central Vietnam [see Fig. 8(e)]. However, the SED values again differ, showing the differences between severe drought and moderate drought. This implies that a 1-standard deviation drought defined by SPI does not necessarily translate into a 1-standard deviation agricultural drought, as identified by root-zone soil moisture-derived SED.

E. Transition From Meteorological Drought to Agriculture Drought Under Humid Conditions

By comparing the black dashed line (SPI) and the lower bar (SED) in Figs. 7(b)–(d) and 8(c)–(e), it is evident that the severest agriculture drought occurs often after the severest of meteorological drought, which consistent with the drought propagation theory—that agricultural droughts are caused by the accumulation of long-term deficiency of precipitation. Such a drought transition process (from meteorological drought to agricultural drought) is longer and more pronounced in wetter regions, which can be considered as a resistance effect of existing soil moisture to meteorological drought.

To investigate the process of drought transition, we selected the area around Tonle Sap Lake, where there is an abundant water system and sufficient soil moisture to prolong the transition process, as the study area. Cambodia was divided into two regions, namely: The Tonle Sap Lake regions [including Tonle Sap Lake and surrounding 100 km regions: Red area in Fig. 9(a)], and Western Cambodia [except Tonle Sap Lake regions: Blue area in Fig. 9(a) subsequently]. We calculated the development of drought area percentage in these two regions. The drought closer to the Tonle Sap Lake region develops later than in the surrounding areas [see Fig. 9(b) and (c)].

The difference may also have a physical and real component. The development of drought in Western Cambodia occurs significantly earlier than in the Tonle Sap Lake region, particularly for moderate droughts that appear on a larger scale almost a month earlier. A possible reason may be that the well-developed irrigation around Tonle Sap Lake, which allows the root-zone soil moisture in its surrounding area to remain relatively abundant during the early stages of drought, is resistant to the occurrence of agricultural drought. This result also indicates the response of SED to topographic features. Notably, the drought resistance of Tonle Sap Lakes detected by SED is also evident in 2017 and 2019.

SED and SPI describe drought from separate perspectives, and it is difficult to compare drought indices directly because the indices always formulated by different hydrometeorological

variables or for different areas [71], [72], but if only from the aspect of guidance for agricultural productivity, SED has the advantage in responding to the actual drought situation. Furthermore, the two indices differ in the classification of drought, for example, the "severe drought," which is a relative rather than absolute concept, varies from centuries to months, single or periodic water deficit, the SED describes the intensity and duration of water deficit in the short term (months or a year) [9], [10], which may be more instructional and meaningful to agriculture.

V. Conclusion

We use surface soil moisture estimates based on microwave remote sensing data to monitor the drought evolution in the Mainland South Asia region. We place agricultural droughts (deficit in root-zone soil moisture and a frequency distribution-based index, SED) in the context of the forcing meteorological drought (deficit in precipitation and frequency distribution-based index, SPI). The analyzes of SPI and SED suggest that SED is a reliable indicator for detecting the onset, evolution, and end of drought events. SED provides a higher temporal resolution than precipitation-based proxies of drought state and can be calculated at a 9 km scale globally without ancillary or historical calibration data. This makes the approach generalizable for near-real-time drought monitoring.

This study also demonstrates the capability for satellite soil moisture to retroactively determine the progression, extent, and severity of recent droughts by following an exceptional agricultural drought event affecting MSA in 2016, which also demonstrates the transition process (soil moisture resistance) from meteorological drought to agricultural drought. However, this study can be further improved in terms of detail and study scale. For example, the time scale parameter T can be determined at the grid-scale based on the characteristics of soil moisture dry-down. In addition, the study can be extended from MSA to a larger area or even globally with further improvement of spatial and temporal resolution of remote sensing data.

References

[1] K. Marvel et al., "Twentieth-century hydroclimate changes consistent with human influence," *Nature*, vol. 569, no. 7754, pp. 59–65, May 2019.

[2] B. Cook, *Drought: An Interdisciplinary Perspective*. New York, NY, USA: Columbia Univ. Press, 2019.

[3] A. Dai, "Increasing drought under global warming in observations and models," *Nature Climate Change*, vol. 3, no. 1, pp. 52–58, Aug. 2013.

[4] A. F. Van Loon et al., "Drought in the anthropocene," *Nature Geosci.*, vol. 9, no. 2, pp. 89–91, Feb. 2016.

[5] W. Wan et al., "A holistic view of water management impacts on future droughts: A global multimodel analysis," *J. Geophys. Res.: Atmospheres*, vol. 123, no. 11, pp. 5947–5972, May 2018.

[6] A. AghaKouchak et al., "Water and climate: Recognize anthropogenic drought," *Nature News*, vol. 524, no. 7566, pp. 409–411, Aug. 2015.

[7] J. Martínez-Fernández et al., "Satellite soil moisture for agricultural drought monitoring: Assessment of the SMOS derived soil water deficit index," *Remote Sens. Environ.*, vol. 177 pp. 277–286, May 2016.

[8] R. Lal et al., "Adapting agriculture to drought and extreme events," *J. Soil Water Conservation*, vol. 67, no. 6, pp. 162A–166A, Nov. 2012.

[9] D. A. Wilhite, "Drought as a natural hazard: Concepts and definitions," in *Drought: A Global Assessment*, vol. 1. London, U.K.: National Drought Mitigation Center, 2000, ch. 1, pp. 3–18.

[10] Z. Hao and V. P. Singh, "Drought characterization from a multivariate perspective: A review," *J. Hydrol.*, vol. 527, pp. 668–678, Aug. 2015.

[11] W. C. Palmer, *Meteorological Drought*, vol. 30. Washington, DC, USA: U.S. Department of Commerce, Weather Bureau, 1965.

[12] W. C. Palmer, "Keeping track of crop moisture conditions, nationwide: The new crop moisture index," *Weatherwise*, vol. 21, pp. 156–161, 1968.

[13] H. Carrão et al., "An empirical standardized soil moisture index for agricultural drought assessment from remotely sensed data," *Int. J. Appl. Earth Observ. Geoinf.*, vol. 48, pp. 74–84, Jun. 2016.

[14] T. B. McKee et al., "The relationship of drought frequency and duration to time scales," in *Proc. 8th Conf. Appl. Climatol.*, 1993, vol. 17, no. 22, pp. 179–183.

[15] B. Narasimhan and R. Srinivasan, "Development and evaluation of soil moisture deficit index (SMDI) and evapotranspiration deficit index (ETDI) for agricultural drought monitoring," *Agricultural Forest Meteorol.*, vol. 133, no. 1–4, pp. 69–88, Nov. 2005.

[16] Y. Qin et al., "Comparative analysis of drought based on precipitation and soil moisture indices in Haihe basin of North China during the period of 1960–2010," *J. Hydrol.*, vol. 526, pp. 55–67, Jul. 2015.

[17] P. Woli et al., "Agricultural reference index for drought," *Agronomy J.*, vol. 104, no. 2, pp. 287–300, Mar. 2012.

[18] J. Sheffield and E. F. Wood, "Projected changes in drought occurrence under future global warming from multi-model, multi-scenario, IPCC AR4 simulations," *Climate Dyn.*, vol. 31, no. 1, pp. 79–105, Nov. 2007.

[19] E. G. Njoku, T. J. Jackson, V. Lakshmi, T. K. Chan, and S. V. Nghiem, "Soil moisture retrieval from AMSR-E," *IEEE Trans. Geosci. Remote Sens.*, vol. 41, no. 2, pp. 215–229, Feb. 2003.

[20] Y. H. Kerr et al., "The SMOS mission: New tool for monitoring key elements of the global water cycle," *Proc. IEEE*, vol. 98, no. 5, pp. 666–687, May 2010.

[21] D. Entekhabi et al., "The soil moisture active passive (SMAP) mission," *Proc. IEEE*, vol. 98, no. 5, pp. 704–716, May 2010.

[22] K. Imaoka et al., "Instrument performance and calibration of AMSR-E and AMSR2," *Int. Arch. Photogrammetry, Remote Sens. Spatial Inf. Sci.*, vol. 38, no. 8, pp. 13–18, 2010.

[23] A. Scaini et al., "SMOS-derived soil moisture anomalies and drought indices: A comparative analysis using in situ measurements," *Hydrological Processes*, vol. 29, no. 3, pp. 373–383, Jan. 2014.

[24] S. Chakrabarti, T. Bongiovanni, J. Judge, L. Zotarelli, and C. Bayer, "Assimilation of SMOS soil moisture for quantifying drought impacts on crop yield in agricultural regions," *IEEE J. Sel. Topics Appl. Earth Observ. Remote Sens.*, vol. 7, no. 9, pp. 3867–3879, Sep. 2014.

[25] D. Liu et al., "Performance of SMAP, AMSR-E and LAI for weekly agricultural drought forecasting over continental United States," *J. Hydrol.*, vol. 553, pp. 88–104, Oct. 2017.

[26] A. Mishra et al., "Drought monitoring with soil moisture active passive (SMAP) measurements," *J. Hydrol.*, vol. 552, pp. 620–632, Sep. 2017.

[27] J. Bai et al., "Assessment of the SMAP-derived soil water deficit index (SWDI-SMAP) as an agricultural drought index in China," *Remote Sens.*, vol. 10, no. 8, Aug. 2018, Art. no. 1302.

[28] S. Sadri, E. F. Wood, and M. Pan, "Developing a drought-monitoring index for the contiguous US using SMAP," *Hydrol. Earth Syst. Sci.*, vol. 22, no. 12, pp. 6611–6626, Dec. 2018.

[29] S. Sadri et al., "A global near-real-time soil moisture index monitor for food security using integrated SMOS and SMAP," *Remote Sens. Environ.*, vol. 246, Sep. 2020, Art. no. 111864.

[30] A. F. Feldman et al., "Land-atmosphere drivers of landscape-scale plant water content loss," *Geophys. Res. Lett.*, vol. 47, no. 22, Oct. 2020, Art. no. e2020GL090331.

[31] R. H. Reichle et al., "Assessment of the SMAP level-4 surface and root-zone soil moisture product using in situ measurements," *J. Hydrometeorology*, vol. 18, no. 10, pp. 2621–2645, Oct. 2017.

[32] C. Albergel et al., "LDAS-monde sequential assimilation of satellite derived observations applied to the contiguous US: An ERA-5 driven reanalysis of the land surface variables," *Remote Sens.*, vol. 10, Oct. 2018, Art. no. 1627.

[33] Y. Sawada, T. Koike, E. Ikoma, and M. Kitsuregawa, "Monitoring and predicting agricultural droughts for a water-limited subcontinental region by integrating a land surface model and microwave remote sensing," *IEEE Trans. Geosci. Remote Sens.*, vol. 58, no. 1, pp. 14–33, Jan. 2020.

[34] S. V. Kumar et al., "The 2019–2020 Australian drought and bushfires altered the partitioning of hydrological fluxes," *Geophys. Res. Lett.*, vol. 48, no. 1, pp. 1–10, Jan. 2021.

[35] Z. Wang and C. Chang, "A numerical study of the interaction between the large-scale monsoon circulation and orographic precipitation over South and Southeast Asia," *J. Climate*, vol. 25, no. 7, pp. 2440–2455, Apr. 2012.
[36] C. Tsai, S. K. Behera, and T. Waseda, "Indo-China monsoon indices," *Sci. Rep.*, vol. 5, no. 1, pp. 1–10, Jan. 2015.
[37] Y. Y. Loo, L. Billa, and A. Singh, "Effect of climate change on seasonal monsoon in Asia and its impact on the variability of monsoon rainfall in Southeast Asia," *Geosci. Front.*, vol. 6, no. 6, pp. 817–823, Nov. 2015.
[38] D. Siingh et al., "Lightning and convective rain over Indian peninsula and Indo-China peninsula," *Adv. Space Res.*, vol. 55, no. 4, pp. 1085–1103, Feb. 2015.
[39] P. Li et al., "A review of swidden agriculture in Southeast Asia," *Remote Sens.*, vol. 6, no. 2, pp. 1654–1683, Feb. 2014.
[40] E. Zaveri et al., "Invisible water, visible impact: Groundwater use and Indian agriculture under climate change," *Environ. Res. Lett.*, vol. 11, no. 8, Aug. 2016, Art. no. 084005.
[41] V. Panyakul, "Organic agriculture in Laos PDR: Overview and development options,' international trade center's project 'Support to trade promotion and export development in Lao PDR," Earth Net Found./Green Net. Int. Trade Center, Geneva, Switzerland, Rep. LAO/61/89, Jan. 2009.
[42] T. D. Vien, "Climate change and its impact on agriculture in Vietnam," *J. Int. Soc. Southeast Asian Agricultural Sci.*, vol. 17, no. 1, pp. 17–21, 2011.
[43] M. Thilakarathne and V. Sridhar, "Characterization of future drought conditions in the lower Mekong River Basin," *Weather Climate Extremes*, vol. 17, pp. 47–58, Sep. 2017.
[44] Y. Trisurat et al., "Basin-wide impacts of climate change on ecosystem services in the lower Mekong basin," *Ecological Res.*, vol. 33, no. 1, pp. 73–86, Oct. 2017.
[45] The Mekong River Commission, Drought Management Strategy for the Lower Mekong Basin 2020-2025, The Mekong River Commission, Vientiane, Laos, Nov. 2019. [Online]. Available: http://www.mrcmekong.org/assets/Publications/MRC-DMS-2020-2025-Fourth-draft-V3.0-for-web_SM.pdf
[46] O. Polpanich, "Drought in Southeast Asia," in *GEO-DRI Drought Monitoring Workshop*. Bangkok, Thailand: Stockholm Environ, Inst. - Asia, May 2010, pp. 10–111.
[47] H. Guo et al., "Meteorological drought analysis in the lower Mekong Basin using satellite-based long-term CHIRPS product," *Sustainability*, vol. 9, no. 6, May 2017, Art. no. 901.
[48] J. L. Sabo et al., "Designing river flows to improve food security futures in the lower Mekong Basin," *Science*, vol. 358, no. 6368, Dec. 2017, Art. no. 1053.
[49] P. E. O'Neill et al., *SMAP Enhanced L3 Radiometer Global Daily 9 km EASE-Grid Soil Moisture, Version 4*. Boulder, CO, USA: NASA Nat. Snow and Ice Data Center Distrib. Act. Arch. Center, 2020, doi: 10.5067/NJ34TQ2LFE90.
[50] R. Gelaro et al., "The modern-era retrospective analysis for research and applications, version 2 (MERRA-2)," *J. Climate*, vol. 30, no. 14, pp. 5419–5454, 2017.
[51] S. Siebert et al., *Global Map of Irrigation Areas Version 5*. Rome, Italy: Rheinische Friedrich-Wilhelms-Univ. Food Agriculture Org. United Nations, vol. 2, pp. 1299–1327, 2013.
[52] T. G. Farr et al., "The shuttle radar topography mission," *Rev. Geophys.*, vol. 45, no. 2, 2007.
[53] E. A. Waraich et al., "Improving agricultural water use efficiency by nutrient management in crop plants," *Acta Agriculturae Scandinavica, Sect. B-Soil Plant Sci.*, vol. 61, no. 4, pp. 291–304, 2011.
[54] L. Ma et al., "Root zone water quality model sensitivity analysis using Monte Carlo simulation," *Trans. ASAE*, vol. 43, no. 4, pp. 883, 2000.
[55] D. J. S. Gianotti et al., "Terrestrial evaporation and moisture drainage in a warmer climate," *Geophys. Res. Lett.*, vol. 47, no. 5, Feb. 2020, Art. no. e2019GL086498.
[56] W. Wagner et al., "A method for estimating soil moisture from ERS scatterometer and soil data," *Remote Sens. Environ.*, vol. 70, no. 2, pp. 191–207, Nov. 1999.
[57] C. Albergel et al., "From near-surface to root-zone soil moisture using an exponential filter: An assessment of the method based on in-situ observations and model simulations," *Hydrol. Earth Syst. Sci.*, vol. 12, no. 6, pp. 1323–1337, Dec. 2008.
[58] D. Entekhabi et al., *SMAP Handbook: Mapping Soil Moisture and Freeze/Thaw From Space*. Pasadena, CA, USA: NASA, Jet Propulsion Lab., 2014, Accessed: Aug. 12, 2021. [Online]. Available: https://soilsensor.com/wp-content/uploads/SMAP_Handbook_FINAL_1_JULY_2014_Web.pdf
[59] J. Hongtao et al., "Extending the SMAP 9-km soil moisture product using a spatio-temporal fusion model," *Remote Sens. Environ.*, vol. 231, Sep. 2019, Art. no. 111224.
[60] R. Sehler et al., "Investigating relationship between soil moisture and precipitation globally using remote sensing observations," *J. Contemporary Water Res. Educ.*, vol. 168, no. 1, pp. 106–118, Dec. 2019.
[61] J. Sheffield et al., "A simulated soil moisture based drought analysis for the United States," *J. Geophys. Res.: Atmospheres*, vol. 109, no. D24, Dec. 2004.
[62] E. Cho, M. Choi, and W. Wagner, "An assessment of remotely sensed surface and root zone soil moisture through active and passive sensors in northeast Asia," *Remote Sens. Environ.*, vol. 160, pp. 166–179, Apr. 2015.
[63] A. Ceballos et al., "Validation of ERS scatterometer-derived soil moisture data in the central part of the Duero Basin, Spain," *Hydrological Processes: Int. J.*, vol. 19, no. 8, pp. 1549–1566, May 2005.
[64] M. Zohaib, H. Kim, and M. Choi, "Evaluating the patterns of spatiotemporal trends of root zone soil moisture in major climate regions in East Asia," *J. Geophys. Res.: Atmospheres*, vol. 122, no. 15, pp. 7705–7722, Aug. 2017.
[65] K. J. Tobin et al., "Multi-decadal analysis of root-zone soil moisture applying the exponential filter across CONUS," *Hydrol. Earth Syst. Sci.*, vol. 21, no. 9, pp. 4403–4417, Sep. 2017.
[66] T. W. Ford, E. Harris, and S. M. Quiring, "Estimating root zone soil moisture using near-surface observations from SMOS," *Hydrol. Earth Syst. Sci.*, vol. 18, no. 1, pp. 139–154, Jan. 2014.
[67] L. Feldman, "The maize root," in *The Maize Handbook*. New York, NY, USA: Springer, 1994, pp. 29–37.
[68] R. A. Ordóñez et al., "Maize and soybean root front velocity and maximum depth in Iowa, USA," *Field Crops Res.*, vol. 215, pp. 122–131, Jan. 2018.
[69] Mekong River Commission, Ministry of Water Resources of China, Joint Observation and Evaluation of the Emergency Water Supplement from China to The Mekong River, Mekong River Commission and Ministry of Water Resources of China, Vientiane, Laos, Rep, Oct. 2016.
[70] S. Eslamian et al., "A review of drought indices," *Int. J. Constructive Res. Civil Eng.*, vol. 3, no. 4, pp. 48–66, Nov. 2017.
[71] A. Pathak et al., "Comparison of two hydrological drought indices," *Perspectives Sci.*, vol. 8, pp. 626–628, Sep. 2016.
[72] K. Jain et al., "Comparison of drought indices for appraisal of drought characteristics in the Ken River Basin," *Weather Climate Extremes*, vol. 8, pp. 1–11, Jun. 2015.

Yishan Li (Student Member, IEEE) received the B.S. degree in water supply and drainage from the South China University of Technology, Guangdong, China, in 2015 and the Ph.D. degree in ecology from Tsinghua University, Beijing, China, in 2021.

His interest in application filed is disaster forecast, such as drought and flood forecasts. And his major include discharge simulation and monitoring by using remote sensing data and distributed hydrological models.

Hui Lu (Senior Member, IEEE) received the B.Eng. degree in hydraulic engineering and the M.Eng. degree in hydrology from Tsinghua University, Beijing, China, in 2000 and 2003, respectively, and the Ph.D. degree in hydrology from The University of Tokyo, Tokyo, Japan, in 2006.

He is currently an Associate Professor with the Department of Earth System Science, Tsinghua University, and a member of the Joint Center for Global Change Studies, Beijing, China. His research interests include application of remote sensing in hydrology and global change study, radiative transfer model development, passive microwave remote sensing of land surface parameters, and land data assimilation.

Dara Entekhabi (Fellow, IEEE) received the B.A. and M.S. degrees from Clark University, Worcester, MA, USA, in 1983 and 1987, respectively, and the Ph.D. degree in civil and environmental engineering from the Massachusetts Institute of Technology (MIT), Cambridge, MA, USA, in 1990.

He is currently a Professor with the Department of Civil and Environmental Engineering and with the Department of Earth, Atmospheric and Planetary Sciences, MIT. He is also the Science Team Lead of the National Aeronautics and Space Administration's Soil Moisture Active and Passive (SMAP) Mission that was launched in January 2015. His research interests include terrestrial remote sensing, data assimilation, and coupled land-atmosphere systems modeling.

Dr. Entekhabi is a fellow of the American Meteorological Society and the American Geophysical Union. He is also a member of the National Academy of Engineering.

Daniel J. Short Gianotti (Member, IEEE) received the B.S. degree in science in mathematics from Harvey Mudd College, Claremont, CA, USA, in 2003 and the Ph.D. degree in geography and environment from Boston University, Boston, MA, USA, in 2016.

He is currently a Postdoctoral with the Department of Civil and Environmental Engineering, Massachusetts Institute of Technology (MIT), Cambridge, MA, USA. His research interest is the processes that link the land surface and atmosphere, with a focus on water, energy, and carbon.

Kun Yang received the B.E. degree in fluid mechanics and machinery and the M.S. degree in environmental hydraulics from the Department of Hydraulic Engineering, Tsinghua University, Beijing, China, in 1994 and 1997, respectively, and the Ph.D. degree in hydrometeorology from the Department of Civil Engineering, University of Tokyo, Tokyo, Japan, in 2000.

His research interests are land surface modeling, data assimilation and climate modeling, with a focus on interactions among atmosphere–hydrosphere–cryosphere–biosphere in the Tibetan Plateau.

Caihong Luo received the M.S. degrees from the Dalian University of Technology, Dalian, China, in 2000.

Her main research interests include pollutant monitoring, environmental monitoring, atmospheric pollutant monitor and control, and environmental pollutant assessment.

Andrew F. Feldman (Member, IEEE) received the B.S. and M.S. degrees in civil engineering from Drexel University, Philadelphia, PA, USA, in 2016 and the M.S. and Ph.D. degrees in civil and environmental engineering from the Massachusetts Institute of Technology (MIT), Cambridge, MA, USA, in 2018 and 2021, respectively.

He is currently a Postdoctoral Program Fellow with NASA Washington, DC, USA. His research interest includes microwave remote sensing applications for land-surface hydrology and plant sciences.

Wei Wang received the B.S. degree in hydrologic science and the Ph.D. degree in ecology from Tsinghua University, Beijing, China, in 2012, and 2017, respectively.

He was a Visiting Scholar with Pacific Northwest National Laboratory, Richland, WA, USA, from June 2015 to July 2016. His main research interests include land surface water cycle simulation and monitoring, especially the integration of remote sensing techniques and distributed hydrological models into the climate change assessment.

Mr. Wang has been a Member of American Geophysical Union (AGU) since 2014.

Ruijie Jiang received the B.S. degree in oceanographic science from Nanjing University, Nanjing, China, in 2020. He is currently working toward the Ph.D. degree in ecology with the Ministry of Education Key Laboratory for Earth System Modeling and Department of Earth System Science, Tsinghua University, Beijing, China.

His main research interest is hydrological modeling.